The Impact of Structural Changes on Learning Capacity in the Fly Olfactory Neural Circuit

Katherine Xie[1,2], Gabriel Koch Ocker[2]

The Pingry School, 131 Martinsville Road, Basking Ridge, NJ 07920[1], Boston University, Boston, MA 02215[2]

Abstract

The *Drosophila* mushroom body (MB) is known to be involved in olfactory learning and memory; the synaptic plasticity of the Kenyon cell (KC) to mushroom body output neuron (MBON) synapses plays a key role in the learning process. Previous research has focused on projection neuron (PN) to Kenyon cell (KC) connectivity within the MB; we examine how perturbations to the mushroom body circuit structure and changes in connectivity, specifically within the KC to mushroom body output neuron (MBON) neural circuit, affect the MBONs' ability to distinguish between odor classes. We constructed a neural network that incorporates the connectivity between PNs, KCs, and MBONs. To train our model, we generated ten artificial input classes, which represent the projection neuron activity in response to different odors. We collected data on the number of KC-to-MBON connections, MBON error rates, and KC-to-MBON synaptic weights among other metrics. We observed that certain MBONs with very few presynaptic KCs consistently performed worse than others in the odor classification task. Certain developmental types of KCs played a larger role in each MBON's output. We performed random and targeted KC ablation and observed that ablating developmentally mature KCs had a greater negative impact on MBONs' learning than ablating immature KCs. This model furthers our understanding of olfactory learning systems, which provide important clues to understanding the learning and memory mechanisms underlying other regions of the nervous system such as the cerebellum and the hippocampus and have broader implications in artificial intelligence and the treatment of neurodegenerative disorders.

1 Introduction

Learning is a fundamental cognitive process, and disorders of learning such as post-traumatic stress disorder and amnesia can be devastating. *Drosophila melanogaster* exhibit learned behaviors including learning sensory associations. The mushroom body (MB) is a brain region known to be involved in associative learning, more specifically olfactory learning and memory (Eichler et al., 2017). The MB is a subject of intense research as its structure is fairly simple. Our MB model consists of three main cell types: projection neurons (PN), Kenyon cells (KC), and mushroom body output neurons (MBON) (Fig. 1A). In the MB network, PNs receive input from olfactory receptor neurons, and the Kenyon cells (KC) receive input from PNs and other KCs. MBONs receive input from KCs, modulatory neurons, and other MBONs (Eichler et al., 2017). The olfactory circuit also bears a striking resemblance to areas of the brain that are involved in learning and memory, such as the hippocampus, and the cerebellum, which is responsible for coordination and motor control (Campbell & Turner, 2010). Therefore, improving our understanding of the mushroom body can advance our understanding of more complex structures in the brain. This knowledge has potential applications in machine learning and treatment for neurodegenerative diseases.

While previous research has focused on the PN-to-KC connectivity within the mushroom body circuit, our research focus is on how the structural changes of the KC-to-MBON connections plays a role in olfactory learning as the synaptic plasticity of the KC-to-MBON synapses is known to play a crucial role in the olfactory learning process in *Drosophila* (Heisenberg, 2003). We have built a computational model of the MB based on connectivity data collected from an electron microscopic reconstruction of the larval *Drosophila melanogaster* mushroom body (Eichler et al., 2017), which encompasses three neuron types including projection neurons (PN), Kenyon cells (KC), and mushroom body output neurons (MBON). To test our model, we use an odor classification-type problem. We carry out several perturbations to our model in our experiments, observing the effect of these changes' on the accuracy and efficiency of this model.

1.1 Foundations of the Model

In an effort to model the biological aspects of the *Drosophila melanogaster* mushroom body, we have taken previously observed biological components and implemented them computationally. Specifically, we used a connectivity matrix of the entire MB network from Eichler et al. (2017) and selected for neurons on the left hemisphere of the fly brain. The neural network model is composed

of PNs, KCs, and MBONs proceeding in that order (Fig. 1A). We did not include any MBONs that lacked presynaptic KC connections.

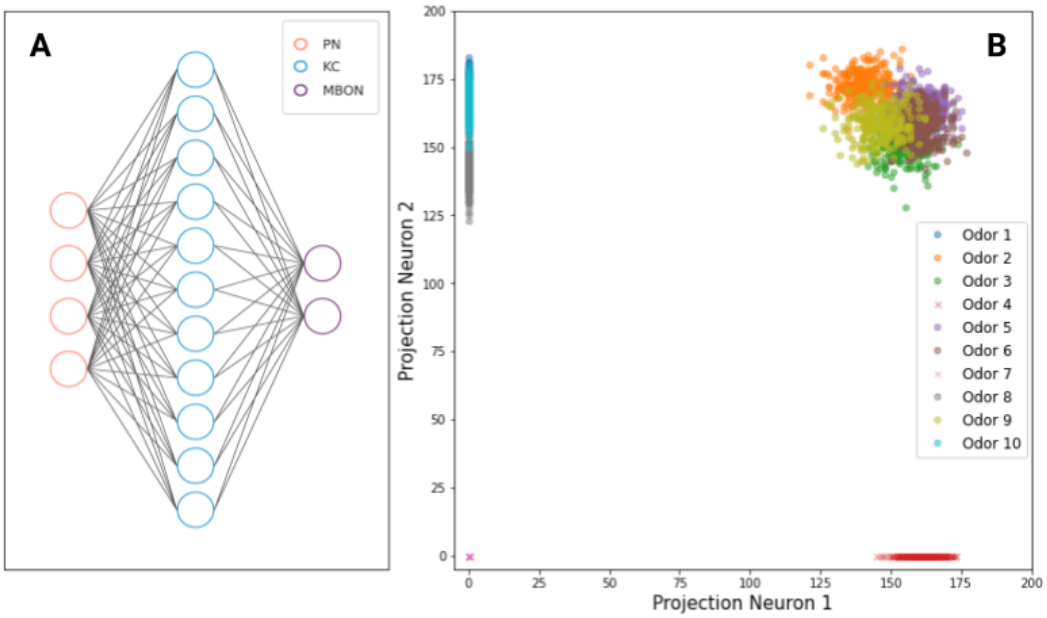

Figure 1. Set up for the computational model of the *Drosophila melanogaster* mushroom body. **A)** An approximation of the mushroom body neural network model composed of 40 PNs, 110 KCs, and 18 MBONs and 1 fictional MBON (added for comparison purposes) that takes in inputs from all KCs in the previous layer. **B)** Distribution of PN activity in response to 10 odors. As there are 40 PNs, PN responses are 40-dimensional; however, only two dimensions are displayed here. Distributions marked with "o" indicate that Projection Neuron 2 fires in response to that odor; distributions marked with "x" indicate that Projection Neuron 2 does not fire in response to that odor. Numbers on the axis represent the number of spikes in response to each odor.

Implemented in Python and Jupyter, our model emulates the biological *Drosophila* MB. Different groupings of PNs are found in the glomeruli of the *Drosophila melanogaster* antenna lobe, and each group of PNs typically will only fire in response to certain odors; this typical response is the odor selectivity of PNs (Wilson, 2013). To model this biological response, we created a binomial probability distribution that implements a coin flip model for whether the PN fires or not in response to each odor (Turner et al., 2008). After receiving a stimulus, responsive PNs fire around 162 spikes per second, whereas a KC will likely spike only one or two times within that time frame (Stevens, 2015). If a PN is responsive to a particular odor, then its spike count on a presentation of that odor is sampled from a binomial distribution with 200 trials and the spike probability r. To model variability in the PN responsiveness to different odors, we sample r from a normal distribution with a mean of 0.8 and standard deviation of 0.05. We repeat these processes to generate 10 separate PN activity distributions, as shown in Figure 1B, in response to the 10 odors we

use as inputs into our computational model. Each point represents the PN response to a sample of one of the 10 odors. Overlaps among the distributions indicate that these odors have similarities in their PN representations.

Based on Figure 1B, PN 2 does not respond to odor 4 (red "x"'s) as the PN 2 spike value is zero. PN 1 does not respond to several odors: odor 1, 3, and 10. A cloud of five odors in the upper right of Figure 1B would be difficult to distinguish based on only the response activity of PN 1 and PN 2. These odor-evoked PN responses drive KC activity, which in turn provides input to the MBONs (Fig. 1A).

To imitate the olfactory learning process in flies, we trained our neural network model on a 10-odor classification task. I assign each MBON a target response, spike or no spike, in response to each odor. Each MBON must produce the correct output of 1 or 0 in response to its odor-evoke KC inputs. Perceptrons, introduced by Rosenblatt (1958), are used to model each KC and MBON in the MB network. Upon receiving an input point, each perceptron will generate an output based on its weights w_i and bias θ:

$$y = \sum_i input_i \times w_i + \theta.$$

Mimicking the 5% KC firing rate in response to an odor, we set the KC bias at a threshold value so that the KC would only fire 5% of the time (Honegger et al., 2011). This models the global inhibition KCs receive from anterior paired lateral neuron (Eichler et al., 2017). At each time step of training, we adjust components of the KC-to-MBON network, including the weights and the bias values, based on the Delta Rule as follows (Widrow & Hoff, 1960):

$$\Delta w_i = error \times input_i \times \alpha,$$

where Δw represents the change in weights and α equals 0.01, the learning rate. The error is the difference between the target and actual output generated by the model. The Delta Rule is applied to the bias values, θ, as well. These adjustments minimize the error in MBON outputs over each time step. Our model was trained for a total of 5,000 time steps, in each of which the model was given a

random input point from any of the 10 PN activity distributions. This training process was repeated for 10 realizations.

2 Results

Our preliminary analysis consists of various metrics such as the performance of different MBONs and the evolution of weights. In Figure 2A, most of the MBONs had learned the classification task fairly quickly by around 200 time steps, although there is some variability. Most notably, however, the learning curves of MBON-o1 (pink) and MBON-n1 (brown) diverge from the rest. MBON-o1 takes almost 400 time steps to learn the task, nearly double the number of time steps of the next slowest MBON. MBON-n1 fails to learn the task, with its error rate (ER) plateauing at around 0.3; this is an instance of a finite training-time effect. Upon further examination, we found that MBON-n1 and MBON-o1 had the two lowest numbers of presynaptic KCs among all the MBONs. These differences in the competency of various MBONs drive our next experiments and analyses, in which we examine how aspects of the KC-to-MBON network's structure influences these diverse results among MBONs.

There are also noticeable differences in how the weights change over time across different MBONs. Two examples of this are depicted in Figure 2B and 2C. The weights over time of MBON-a2 continue changing for over 200 time steps, whereas the weights of MBON-b1 cease to change after ~50 time steps. In addition to the accuracy of different MBONs, another consideration in our experiments is how efficiently each MBON learns the task. Between these two MBONs, MBON-b1 learns considerably faster.

Continuing examinations into the weights of this model, we looked at how weights change after training. I noticed that, for many KCs, there are differences in both the center and the spread between final and initial output weight distributions. The final weight distribution of this particular 1 claw KC has a greater spread than the initial distribution, and the center does not change significantly (Figure 2D). Figure 2E shows that, after training, the final weight distribution of this 2 claw KC increases in spread and shifts to the left. In other words, the weights' variability increases, and their values decrease overall. The resulting weight distribution of the 2 claw KC's weights differ from the 1 claw KCs in this respect as the weight values of the 1 claw KCs do not change greatly.

The 5 claw KC's final weight distribution (Figure 2F) does not vary greatly from its initial distribution. With only a few weight values shifting negative, the spread increases minimally.

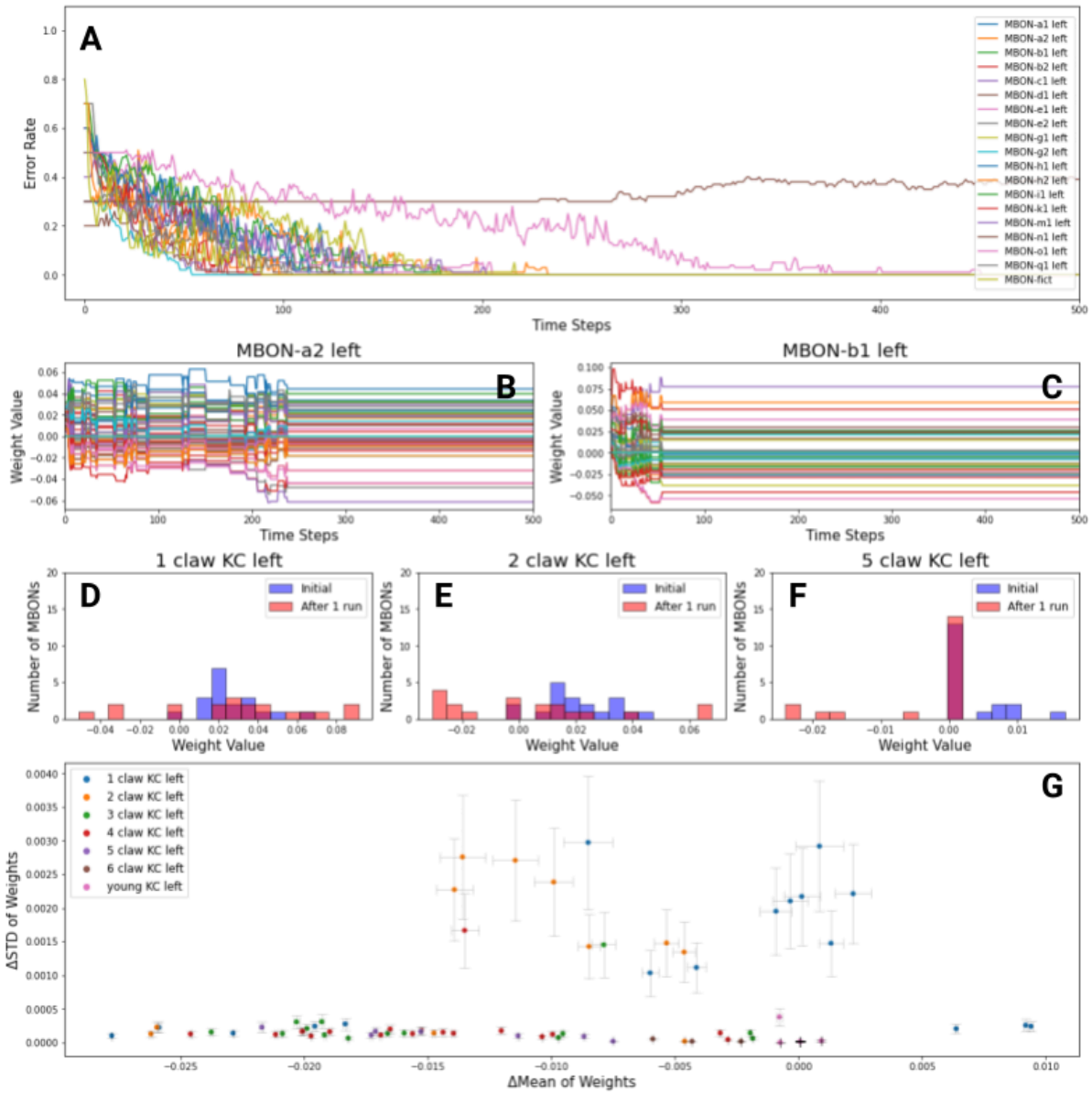

Figure 2. Results of training the model and training's effect on components of the model. **A)** Average ER over time across 10 realizations for all 19 MBONs. **B & C)** Weights over time of MBON-a2 and MBON-b1, respectively. Each line represents the changing weight value of a synaptic connection from an MBON's presynaptic KC. **D, E & F)** Initial and final (after 1 realization of training) weight distributions of a 1 claw KC, 2 claw KC, and 5 claw KC, respectively, across all MBONs. The magenta color indicates where the initial and final weight distributions overlap. **G)** Scatter plot of the average across realizations of the change in standard deviation of weights vs. change in mean of weights. Δ is the change in final weights from the initial set of weights. The seven different KC types are labeled by color.

From the summary scatter plot in Figure 2G, the distinct cluster of the 1 claw KC and 2 claw KC is clear. The cluster of 1 claw KC points (blue) are distributed around a ΔMean of 0; therefore, the average weight value of 1 claw KC is typically stable. However, these points have a positive ΔSTD, so the spread of weight values increases on average. The rest of the KC types, 3 to 6 claw and young KCs, do not appear to experience an increase in the spread of their weight values; most weight values for these KCs also decrease. These differing results between KCs raise other questions about the different role and level of influence that each KC type has.

In the biological mushroom body, KCs that have fewer claws are typically more developmentally mature (Eichler et al., 2017). These older KCs, we hypothesize, are more involved in the olfactory circuit's ability to learn; younger KCs that have not fully developed are less involved. To test this, we will ablate KCs and measure the impact of this ablation on the model MBONs' ability to learn the odor classification task. As we found that KCs with fewer claws had higher final weights onto the MBONs, our prediction is that ablating these more mature KCs will affect MBON performance more than ablating those that are younger and have lower weights.

2.1 Ablation Experiments

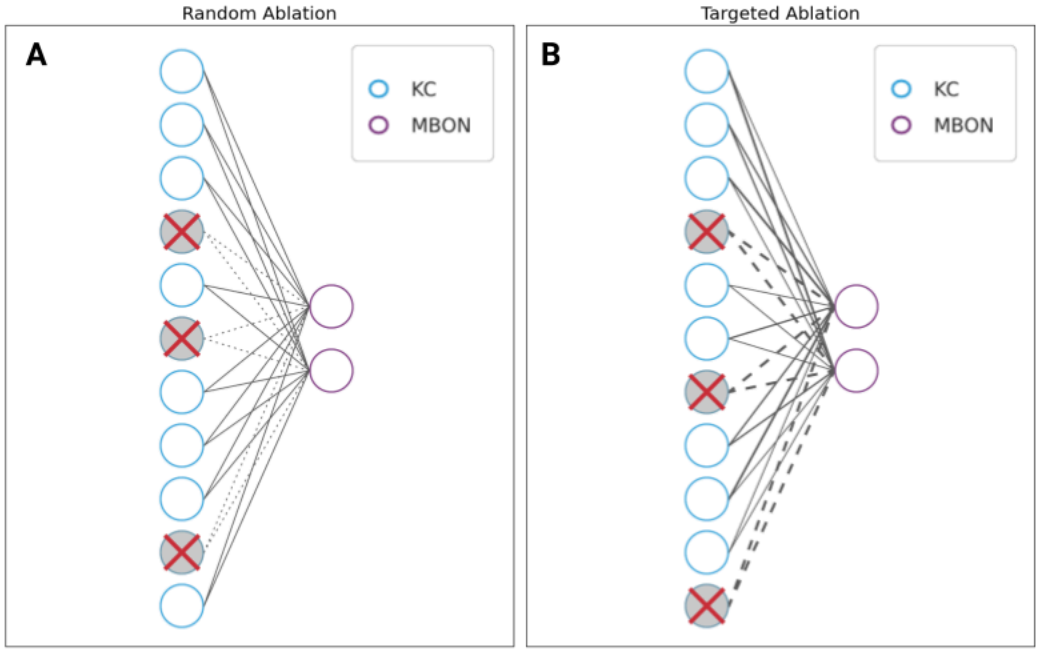

Figure 3. Visualization of random and targeted ablation procedures. KCs marked with an "x" have been ablated. Solid lines between nodes indicate that there exists a synaptic connection. Dotted lines mark the absence of a synaptic connection. **A)** Random ablation of KCs. A certain number of KCs are randomly

selected for ablation, meaning any of their postsynaptic connections to MBONs are removed. **B)** Targeted ablation of KCs. A certain number of KCs are removed based on their total strength of synaptic connections, where line thickness represents the synaptic weight value. KCs with the highest sum of synaptic weight values are ablated first in targeted ablation.

To further explore the observed differences between KCs and MBONs, we performed two types of ablation experiments: random ablation and targeted ablation. When a KC is ablated, we completely remove that KC from the network by setting all of its synaptic connections to a weight of zero. In targeted ablation, KCs are removed from the network based on their total absolute synaptic weight output (Figure 3B). KCs with greater total weight values will be ablated first; for example 1 claw KC would be ablated before 5 claw KC and 2 claw KC (Figure 2D-F). We perform these two experiments to test the effect that structural perturbations have on the performance of the model. We also seeked to determine the level of influence that synaptic connection strength has on the model's performance.

From these two experiments, we collected various metrics and compared the resulting performances of different MBONs after each type of ablation. Figures 4A-C show the ER over 1000 time steps after random ablation of different numbers of KCs. As the number of KCs ablated increases from 1 to 10 to 70, more MBONs take more time steps to learn the task or fail to learn the task. The learning curves of MBON-o1 (pink) and MBON-n1 (brown) consistently take longer to learn the task or plateau at a certain ER; this halt in learning can be attributed to the finite training-time effect. Figures 4D-F also show the ER over 100 time steps after targeted ablation. As the number of KCs ablated increases from 1 to 70, more MBONs fail to learn the task. The MBONs that are quicker to fail are more sensitive to ablation. With 70 KCs removed, almost all MBONs, except for the fictional MBON (Figure 1A), do not learn at all (Figure 4F). The progression to less MBONs learning as the number of KCs removed increases is quicker for targeted ablation than random ablation.

Figure 4G and 4H confirm the above observed pattern. In the random ablation experiment, most of the MBONs' final ERs did not start to increase until 75 KCs were removed from the model (Figure 4G). Only MBON-o1, MBON-k1, and MBON-n1 do not follow this pattern. MBON-n1's negative final ER can be attributed to the method we calculated the difference in final ERs by subtracting the control's (KCs removed = 0) final ER of each MBON from the final ERs after each run in which KCs were removed. As MBON-n1's control final ER was greater than its final ER at 40, 55, and 80 or more KCs removed, the ER in relation to the control is negative. We discovered the three

MBONs whose ERs increased sooner also had less presynaptic KCs; thus, during ablation, their KCs with presynaptic connections are more likely to be completely ablated. Once all 110 KCs were removed, the final ERs seem to converge to several values. This result is due to the way outputs of our model are defined. For example, an MBON with a final ER of 0.8 identifies only 2 out of the 10 odors correctly. Therefore, the ERs with all KCs removed will be constant as MBONs can't learn with no inputs.

In contrast to the random ablation experiment, most MBONs' final ERs begin to increase at 20 KCs removed rather than 75. The final ER of most MBONs begin to plateau at 60 KCs, meaning they can no longer learn the task. This trend indicates that the total synaptic weight value of each KC must be an important factor. Most KCs with high synaptic weight values for each MBON have likely been ablated by that point. Only MBON-fict continues to learn, which makes sense since it still has presynaptic KCs that have not been removed yet (Figure 4H). Overall, targeted ablation had a greater impact on the MBONs' ability to learn to distinguish between odors.

From the varying weight distributions in Figure 4D-F and the greater impact of targeted ablation, we observed that certain KCs play a greater role in allowing the olfactory circuit to learn. We analyzed the differences between KC types and found that during targeted ablation the KCs with a lower number of claws were often removed first (Figure 4I & 4J). When 1 KC is removed, it is a 3 claw KC that is removed, meaning it has the highest total synaptic strength. When 10 KCs are removed, 70% of the KCs removed are 1 claw KCs. Since the total number of each KC varies greatly, we normalize the number of KCs ablated based on their total population (Figure 4J). A clear descending trend emerges: at 50 KCs ablated in particular, we observe that 100% of the single-claw KCs are removed, and next 80% of 2 claw KCs are ablated and then 70% of 3 claw KCs are ablated. This pattern continues. 0% of the 6 claw KCs and young KCs are removed as they have lower total synaptic weight outputs. These KCs removal only increases the final ER minimally, if at all (Figure 4H), indicating that these KCs have less influence over the MBONs' output.

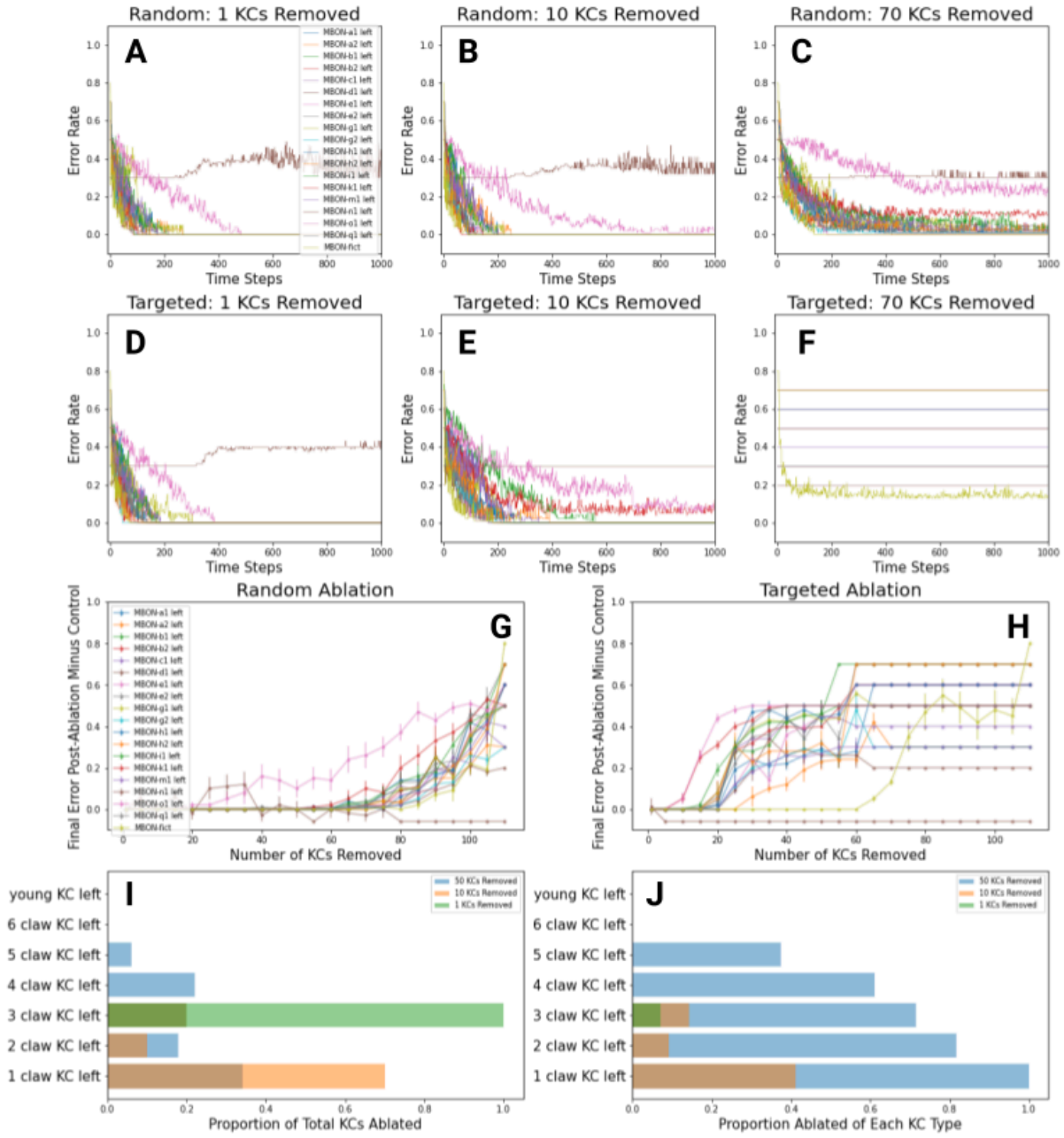

Figure 4. Results of the random and targeted ablation experiments. **A, B, C)** ER over time across MBONs for 1 KC, 10 KCs, and 70 KCs, respectively, removed during random ablation. **D, E, F)** ER over time across MBONs for 1 KC, 10 KCs, and 70 KCs, respectively, removed in targeted ablation. **G)** Average final ER after random ablation in relation to the average final ER in the control (0 KCs removed). ERs are averaged over 10 realizations of training. **H)** Average final ER after random ablation in relation to the average final ER in the control (0 KCs removed). **I)** Bar graph of proportion of total KCs ablated organized into categories of KC type. **J)** Bar graph of proportion ablated of each type of KC organized into categories of KC type. Both **I** and **J** display the proportion of KCs removed for 1, 10, and then 50 KCs removed.

According to Eichler et al. (2017), single-claw KCs are known to be more developmentally mature than other KC types (Eichler 2017). Ablating these single-claw KCs had a greater negative impact on the model's learning capabilities (Fig. 4H & 4J). The results of the random and targeted ablation confirm the hypothesis that KCs with fewer claws are more involved in MBONs' ability to learn the odor classification task. These mature KCs have been integrated into a network that is structured for associative learning.

3 Conclusion

In this report, we have detailed the biological basis of our model and how different structural features impact olfactory training as well as their roles in olfactory learning performance. The results of this study suggest several paths for future research. Building upon the ablation experiments, we could further look at the ablation of specific types of KCs. This ablation would allow us to evaluate the relative importance of different KC types that we begin to examine in our current research. Another direction would involve conducting KC pruning experiments, in which individual KC synaptic connections are removed. Both pruning and ablation experiments have biological origins as neuronal apoptosis and synapse removal occur in the brain. Finally, further adjustments can be made to the model based on its biological equivalent, such as introducing recurrent synaptic connections and inhibitory interactions. To conclude, our computational model of the *Drosophila melanogaster* mushroom body circuit can be used in various ways to further investigate the effect of structural changes in the neural network on olfactory learning and memory as well as, more generally, the neural basis of cognitive function.

In a broader context, our findings on the olfactory circuit's connectivity can aid our understanding of the inner workings of neuroplasticity. The mechanisms of the olfactory system and its plasticity are an important area of study as the loss or reduction of olfactory senses is often one of the first symptoms of neurodegenerative diseases such as Azheimer's and Parkinson's. The link between one's sense of smell and memory is critical as well (Aguilar martínez, 2018). Other researchers and companies have looked into olfactory training as a method to help patients recover their olfactory sense and slow the progression of the neurodegenerative diseases. Kollndorfer et al. (2014) found that olfactory training actually improved neuroplasticity in these patients. Thus, our understanding of neuroplasticity through the structure of olfactory systems can have far-reaching clinical implications.

In the field of artificial intelligence, the bulk of current machine learning algorithms were based on the structure of the visual cortex. However, scientists are now also turning to the olfactory system for fresh inspiration, as its structure has similarities to other more complex regions of the brain such as the hippocampus which is implicated in learning and memory. The nature of odors themselves are random and variable, so understanding how the olfactory circuit processes this information can lead to new machine learning techniques based on olfaction. Research has also proven the inherent generalization ability of the olfactory learning systems is far superior to that of the visual cortex (Huerta & Nowotny, 2009). The olfactory circuit has the potential to adapt to different forms of learning, and could provide insights into how more complex cognitive features of the brain can be integrated into AI.

Bibliography

Eichler, K., Li, F., & Litwin-Kumar, A. *et al.* (2017). The complete connectome of a learning and memory centre in an insect brain. *Nature*, *548*(7666), 175-182. https://doi.org/10.1038/nature23455

Campbell, R. A.a., & Turner, G. C. (2010). The mushroom body. *Current Biology*, *20*(1), R11-R12. https://doi.org/10.1016/j.cub.2009.10.031

Heisenberg, M. (2003). Mushroom body memoir: From maps to models. *Nature Reviews Neuroscience*, *4*(4), 266-275. https://doi.org/10.1038/nrn1074

Wilson R. I. (2013). Early olfactory processing in Drosophila: mechanisms and principles. *Annual review of neuroscience*, *36*, 217–241. https://doi.org/10.1146/annurev-neuro-062111-150533

Turner, G. C., Bazhenov, M., & Laurent, G. (2008). Olfactory representations by drosophila mushroom body neurons. *Journal of Neurophysiology*, *99*(2), 734-746. https://doi.org/10.1152/jn.01283.2007

Stevens, C. F. (2015). What the fly's nose tells the fly's brain. *Proceedings of the National Academy of Sciences*, *112*(30), 9460-9465. https://doi.org/10.1073/pnas.1510103112

Rosenblatt, F. (1958). The perceptron: A probabilistic model for information storage and organization in the brain. *Psychological Review*, *65*(6), 386-408. https://doi.org/10.1037/h0042519

Honegger, K. S., Campbell, R. A. A., & Turner, G. C. (2011). Cellular-Resolution population imaging reveals robust sparse coding in the drosophila mushroom body. *Journal of Neuroscience*, *31*(33), 11772-11785. https://doi.org/10.1523/JNEUROSCI.1099-11.2011

Widrow, B., & Hoff, M. E. (1960). Adaptive switching circuits. *1960 I.R.E Wescon Convention Record*, 96-104.

Aguilar martínez, N., Aguado carrillo, G., Saucedo alvarado, P.e., Mendoza garcía, C.a., Velasco monroy, A.l., & Velasco campos, F. (2018). Clinical importance of olfactory function in neurodegenerative diseases. *Revista Médica Del Hospital General De México*, *81*(4), 268-275. https://doi.org/10.1016/j.hgmx.2017.05.007

Kollndorfer, K., Kowalczyk, K., Hoche, E., Mueller, C. A., Pollak, M., Trattnig, S., & Schöpf, V. (2014). Recovery of olfactory function induces neuroplasticity effects in patients with smell loss. *Neural Plasticity*, *2014*, 1-7. https://doi.org/10.1155/2014/140419

Huerta, R., & Nowotny, T. (2009). Fast and robust learning by reinforcement signals: Explorations in the insect brain. *Neural Computation*, *21*(8), 2123-2151. https://doi.org/10.1162/neco.2009.03-08-733